



An Effective Semantic Mathematical Model for Skin Cancer Classification Using a Saliency-based Level Set with Improved Boundary Indicator Function

Sukesh Hoskote Aswathanarayana^{1*}

Sundeep Kumar Kanipakapatnam²

¹*Department of Computer Science & Engineering, S.E.A. College of Engineering & Technology, Bengaluru, India*

²*Department of Computer Science & Engineering, Geethanjali Institute of Science & Technology, Nellore, India*

* Corresponding author's Email: sukesh.seacet@gmail.com

Abstract: Skin cancer is one of the most commonly occurring cancer and it causes hundreds to thousands of yearly deaths worldwide. Early identification of skin cancer significantly increases the recovery chances from skin cancer. However, precise skin cancer classification is a challenging task because of the ineffective segmentation of skin cancer. In this paper, the saliency-based level set with an improved boundary indicator function (SLSIBIF) is proposed for the effective segmentation of skin cancer. An improved boundary indicator function is used in the segmentation to detect the skin cancer boundaries even under the constraints of low intensity and illumination. The features from the segmented images are extracted by using the GoogLeNet which uses sparse connections to extract an optimal feature. Further, the classification is done using a multi-class support vector machine (MSVM). The performances of the proposed SLSIBIF-MSVM are evaluated using accuracy, sensitivity, specificity, positive predictive value (PPV), error rate, jaccard, and dice coefficient. The existing approaches such as deep-learning system (DLS), ResNet-50, K-means with grasshopper optimization algorithm (GOA) and Region-based CNN (RCNN) and Fuzzy K-means (FKM) are used to compare the SLSIBIF-MSVM. The classification accuracy of SLSIBIF-MSVM for ISIC-2017 dataset is 98.74%, which is high when compared to the DLS, ResNet-50, K means GOA and RCNN-FKM.

Keywords: GoogLeNet, Multi-class support vector machine, Saliency-based level set with improved boundary indicator function, Segmentation, Skin cancer classification.

1. Introduction

The statistics are given by the World Health Organization state that 9.6 million people died because of cancer in 2018. One of every six deaths is occurred because of cancer and it is the world's second cause of mortality. Skin cancer is one of the most common illnesses found in more than 40% of other cancer types [1]. The different factors that provoke skin cancer are viruses, allergies, infections, alcohol usage, smoking, environmental variation, physical activity, exposure to ultraviolet (UV) light, and so on. The UV ray radiation from the sun destroys the DNA that exists in the skin cells. Moreover, the uncommon swellings occurred in the human body also create skin cancer [2, 3, 4]. Different types of skin cancer usually accompanied by basal cells, squamous cells, and melanocytes are

basal cell carcinoma, squamous cell carcinoma, and melanoma respectively. But, Melanoma is one of the rapidly growing skin cancer and it causes around three-fourths of all skin cancer-relevant deaths [5, 6] [7]. The treatment for skin cancer is possible when it is diagnosed in its primary stages [8]. Hence, primary detection, timely analysis and treatment and avoiding the reappearance of skin malignant cancers are very essential for improving the prediction and enhancing survival percentage and patient's quality of life [9, 10, 11].

A manual examination of skin cancer using the naked eye is time-consuming as well as it is imperfect. Moreover, Dermoscopy is the recent noninvasive approach used to identify cancer with improved accuracy. However, none of the above approaches are considered, because of higher time consumption. Hence, computer-aided diagnosis (CAD) is mandatory in the field of medical imaging [12]. The

idea of machine learning is used to minimize human interaction for predicting information, because of the development in programming and technology. This machine learning is used in different applications such as segmentation, classification and so on [13]. The identification and localization of skin lesions are essential to computing the feature of images for diagnosing cancer. The boundary irregularity, higher diameter, and color features of lesions are precisely identified based on the accurate detection of the boundary of the lesion. Initially, the lesion boundaries are obtained using image segmentation while detecting skin cancer. The dissemination of the texture and color is distinguished against the texture color image. Therefore, skin cancer is detected in its early stages by using the segmentation process [14]. However, segmentation is difficult, due to the main differences in the size and position of skin lesions. The differentiation of adjacent tissue cells is affected because of the image's poor contrast. Further, the constraints like ruler mark, color illumination, blood vessel, hair, air bubbles, and ebony frame creates a high level of difficulty during the segmentation [15].

The contributions are concise as follows:

- An effective segmentation using SLSIBIF is developed for segmenting the multi-class skin cancer portions from the image. The SLSIBIF is the combination of saliency and LSF with an improved boundary indicator. The saliency is combined with LSF because saliency required the boundary indicator and LSF required information about specific cancer's form. Moreover, an improved boundary indicator is used to overcome the issues related to illumination and low intensity.
- From the segmented images, the GoogLeNet is used to extract the features whereas sparse connections are used to eliminate the irrelevant features. Next, the MSVM is used to classify the multiple classes of skin cancer.

The rest of the paper is arranged as follows: section 2 provides explanations about existing works done in skin cancer classification. A detailed explanation of SLSIBIF-MSVM-based skin cancer classification is given in section 3. The outcomes of SLSIBIF-MSVM are provided in section 4 whereas the conclusion is provided in section 5.

2. Related Work

Teodoro [16] presented the architecture of convolutional neural networks (CNN) namely

efficient attention net for classifying skin lesions. The hair around the skin cancer was eliminated during the pre-processing and generative adversarial networks (GAN) were used to create the synthetic images. The generation of the synthetic image was used for balancing the number of samples in the training set. Next, the mask for regions of interest in the skin cancer images was formed by using the U-net followed by the classification which was performed using the efficient attention net. The GAN-based synthetic image generation increased the classification performances, because of the balanced images in each class. If the hair was existing in the lesion images, the developed CNN also focused on the features of hair which led to affected the classification.

Khoulood [17] developed a deep-learning system (DLS) for detecting melanoma. Specifically, the two deep learning architectures such as W-net and Inception-Resnet were developed for solving the issue of segmentation and classification. The W-net has three different architectures a ResNet encoder-decoder, a ConvNet encoder-decoder and a feature pyramid network. The utilization of two concatenated architectures of encoder-decoder was used to enhance the segmentation. On the other hand, the classification was highly robust due to the integration of the inception resnet block with a residual neural network.

Al-Masni [18] presented the deep learning architecture to diagnose skin lesions. The developed deep learning integrated boundary detection using deep segment and classification using the deep classifier. The deep segment namely full resolution convolutional networks (FrCN) was used to segment the skin lesion from the dermoscopy images. Next, CNN i.e., ResNet-50, Inception-v3, DenseNet-201 and Inception ResNet-v2 was used to classify the skin lesion using the segmented images. The classifier was enabled to study only certain skin lesion features and representations that avoided the adjacent normal tissue regions. The ResNet-50 was taken as a primary choice due to its performances whereas the InceptionResNet-v2 was considered as a second best for diagnosing skin lesions. The developed two-stage cascade architecture required the preparation of data in each stage.

Thapar [19] developed the K-means with grasshopper optimization algorithm (GOA) for precise detection of foreground regions of skin lesions. Next, the features are extracted using SURF and an appropriate feature subset was chosen using the GOA. Further, the classification of the skin lesion was done using a CNN. The searching capacity of

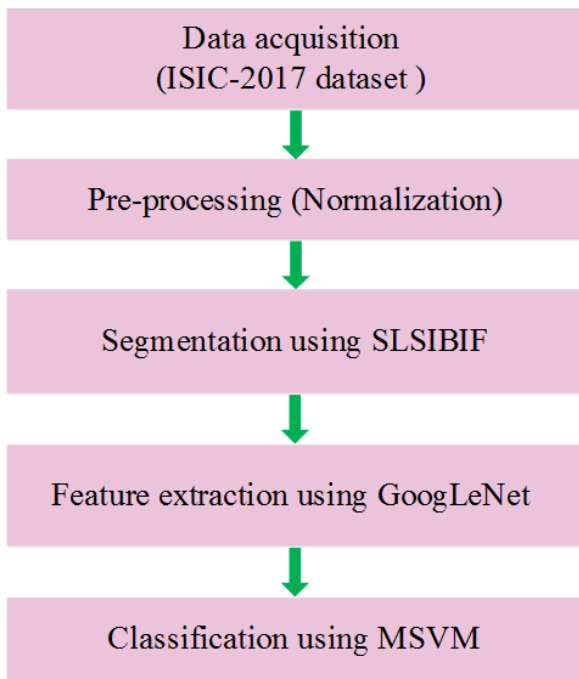


Figure. 1 Block diagram of the SLSIBIF-MSVM method

GOA was used to minimize the pixel mixing issue of the K-means approach. However, the accuracy of the K-means with GOA and CNN was high, only when it was processed with a huge amount of samples.

Nawaz [20] presented the Region-based CNN (RCNN) and Fuzzy K-means (FKM) clustering to perform the automated classification of skin melanoma. At first, the noise and illumination issues were removed for improving the visual information. Next, the FKM was used for segmenting the skin lesions with different sizes and boundaries which was used to classify the melanoma. The developed RCNN with FKM provided an effective classification even under the overfitting issue.

3. SLSIBIF-MSVM method

The proposed skin cancer classification integrates the Saliency-based level set with an improved boundary indicator function to extract the boundaries of skin cancer from the normalized images. Next, an appropriate feature from the segmented images is obtained by using GoogLeNet. Further, an MSVM is used to classify the type of skin cancer according to the features received from the GoogLeNet. Fig. 1 shows the block diagram of the SLSIBIF-MSVM method.

3.1 Dataset acquisition and preprocessing

The ISIC-2017 dataset [21] used in this proposed method is presented by the International Symposium on Biomedical Images (ISBI). This ISIC-2017

dataset has a total of 2750 images which includes three different classes such as nevus, seborrheic keratosis, and melanoma skin cancer classes. The input images from ISIC-2017 are given to the normalization where the pixel intensity of input images is improved by varying the pixel range as shown in Eq. (1).

$$I' = (I - \min) \frac{\text{newmax} - \text{newmin}}{\text{max} - \min} + \text{newmin} \quad (1)$$

Where the input image is denoted as I ; maximum and minimum intensities of I are max and min ; I' denotes the preprocessed image with intensity values of newmin and newmax .

3.2 Segmentation using Saliency-based level set with improved boundary indicator function (SLSIBIF)

In this proposed method, an effective segmentation using SLSIBIF is accomplished for improving the classification. The pre-processed images from normalization are given as input to the SLSIBIF for segmentation. The conventional saliency based segmentation approach segment the image by generating the map according to the color and texture. But, identification of the accurate cancer portion boundary using saliency based segmentation is affected because of the low intensity. On the other hand, the level set function (LSF) detects the boundary without any color and texture information. But, the segmentation using LSF is affected due to the illumination issue. Specific cancer form information is required for LSF and boundary indicator function is required for saliency, therefore both the LSF and saliency are combined in this research namely SLSIBIF. Moreover, the conventional LSF uses an edge detector function, but this function failed to detect accurate boundaries because of illumination and low-intensity issues. Therefore, an improved boundary indicator function is used for predicting the accurate boundary of skin cancer. A contour is integrated as zero level set of LSF. Consider, the φ is the LSF determined on the domain Ω . The Ω_0 ($\varphi = 0$) is defined as a zero level set, Ω_{in} ($\varphi < 0$) is defined as a domain inside Ω_0 and the domain outside Ω_0 is defined as Ω_{out} ($\varphi > 0$). Eq. (2) denotes the energy function $E(\varphi)$.

$$E(\varphi) = \varepsilon_{img}(\varphi, g_\rho) + \varepsilon_{reg}(\varphi, g_\rho) \quad (2)$$

Where external energy is denoted as ε_{img} that is defined by using the image attribute; a regulation term that describes the internal energy utilized as

level set evolution's constraint and edge detector is denoted as g_ρ that is expressed in Eq. (3).

$$g_\rho = \frac{1}{1 + \frac{1}{2}(1 - |\nabla I_\sigma|^2 / \rho^2)(|\nabla I_\sigma|^2 / \rho^2)} \quad (3)$$

Where, the Gaussian filter-based image smoothing using standard deviation σ is denoted as I_σ ; boundary threshold function is denoted as ρ which is obtained by the image's standard deviation S for realizing the adaptive stopping speed. The boundary threshold function is expressed in Eq. (4).

$$\rho(I) = \frac{1 + \sqrt{S(I_\sigma)}}{3} \quad (4)$$

The derived edge detector i.e., boundary indicator function is used in the gradient descent expression shown in Eq. (5) which has three different parts. The 1st part defines the distance regularized term used to eliminate the re-initialization. The 2nd part offers a long term for driving the zero-level set approach for the boundaries of the target. Further, the last term is the area term which is created by the region growing matrix and boundary indicator function. The 3rd part is used for improving the region energy between the neighbor targets and increasing the rate of evolution.

$$\frac{\partial \varphi}{\partial t} = u \operatorname{div}(d_p(|\nabla \varphi|) \nabla \varphi) + \lambda \delta_\varepsilon(\varphi) \operatorname{div}\left(g_\rho \frac{\nabla \varphi}{|\nabla \varphi|}\right) + (\alpha g_\rho + mY) \delta_\varepsilon(\varphi) \quad (5)$$

Where, the weight coefficients that control each parameter effect are denoted as u, λ, α and m ; parameter used to compute the divergence which is denoted as $\operatorname{div}(\cdot)$; LSF's gradient that is received by the gradient operator is denoted as ∇ and Dirac function is denoted as δ_ε which is denoted in Eq. (6).

$$\delta_\varepsilon(\varphi) = \begin{cases} \frac{1}{2\varepsilon} \left(1 + \cos\left(\frac{\pi\varphi}{\varepsilon}\right)\right) & |\varphi| \leq \varepsilon \\ 0 & |\varphi| > \varepsilon \end{cases} \quad (6)$$

Where the δ_ε is acquired from the Heaviside function. The Dirac function is useful only when it is processed in conjunction with the integral. The boundary indicator's line integral with the active contour is calculated by adding the Dirac function because this Dirac function obtains the boundary adjacent to the zero level set. Next, the external energy is attained and determines the contour as a part of the evolution stimulus. The function is affected by the parameter ε used in the Dirac function. The ε is required to be large, when it is necessary to

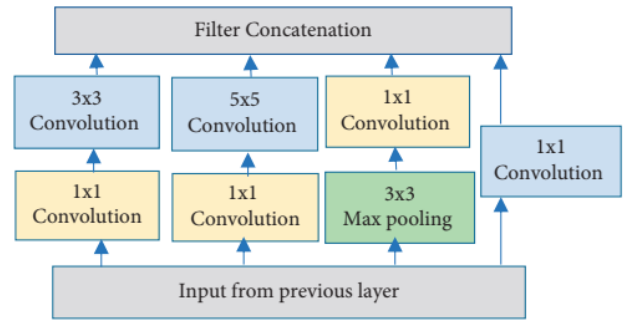


Figure. 2 Architecture of GoogLeNet



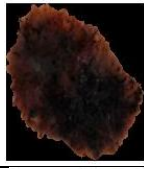
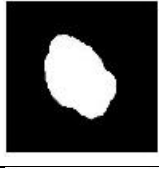
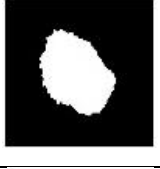
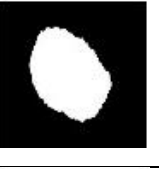
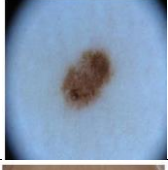


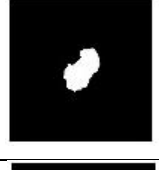
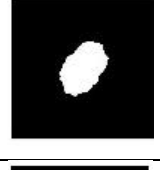
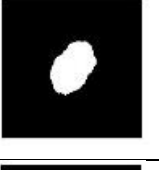

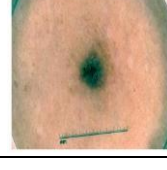

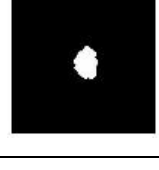
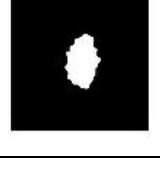

increase the contour's capturing range, however larger ε affects the accuracy of the detected contour. Therefore, generally, ε is chosen as 1.5.

3.3 Feature extraction using GoogLeNet

The segmented images from the SLSIBIF are given as input to the GoogLeNet architecture. The developed GoogLeNet-based feature extraction is used to extract the appropriate features to classify the skin lesions as nevus, seborrheic keratosis, and melanoma. GoogLeNet is a CNN-based structure that is developed by researchers of Google. The GoogLeNet is created according to the inception architecture which includes a multiscale convolutional transformation using split, transform, and merge concepts. Fig. 2 shows the common approach of the inception block.

The inception block is diverse from other deep learning approaches where it has a constant convolution size for each layer. The convolutions of 1×1 , 3×3 and 5×5 and max pooling of 3×3 are accomplished in a parallel manner in the input and output of these operations are loaded together for generating the final output. The typical convolutional layers are swapped with small blocks in GoogLeNet. These blocks have condensed filters in various sizes e.g., 1×1 , 3×3 and 5×5 for acquiring the spatial information at various scales which comprises the levels of both fine and coarse grain. Next, numerous convolutions with 1×1 , 3×3 , and 5×5 filters and 3×3 max-pooling layers are arranged in the GoogLeNet. The incorporation of the bottleneck layer of 1×1 convolutional filters before the huge-size kernels is used to control the GoogLeNet. The number of parameters such as biases and weights of the structure is minimized by using the 1×1 convolution. Additionally, unwanted feature maps are avoided by using sparse connections.

Table 1. Segmented image of skin cancer

Classes of skin cancer	Original image	Normalized image	Segmented image	Saliency level set	SLSIBIF method (Ground truth)	Original Ground truth
Melanoma						
Nevus						
Seborrheic keratosis						

3.4 Classification using MSVM

The MSVM processes the features obtained from the GoogLeNet for classifying it into nevus, seborrheic keratosis and melanoma skin cancer classes. In general, the typical Support Vector Machine (SVM) is made to perform binary classification. Next, the one-against-one is used in SVM to turn it into MSVM [22] for classifying the multiple types of skin cancers. The nonlinear issues are overcome by using the radial basis function as the kernel in MSVM

4. Results and discussion

The results of skin cancer segmentation and classification using the proposed method are provided in this section. The proposed method is implemented and simulated using MATLAB R2020a software. The system used to analyze the proposed method is configured with 16GB RAM and an i7 processor. The ISIC-2017 dataset is used for evaluating the proposed method where k-fold validation is performed for evaluating different splits of data. Here, the value of k is set as 5 during the analysis. The segmentation using the SLSIBIF is analyzed using jacard, dice coefficient, accuracy and sensitivity whereas the classification using overall SLSIBIF-MSVM is analyzed using accuracy, sensitivity, specificity, Positive Predictive Value (PPV) and error rate. The expressions from Eq. (7) to Eq. (13) are used to compute the performance parameters.

$$Accuracy = \frac{TP+TN}{TN+TP+FN+FP} \times 100 \quad (7)$$

$$Sensitivity = \frac{TP}{TP+FN} \times 100 \quad (8)$$

$$Specificity = \frac{TN}{TN+FP} \times 100 \quad (9)$$

$$PPV = \frac{TP}{TP+FP} \times 100 \quad (10)$$

$$Error\ rate = 100 - Accuracy \quad (11)$$

$$Dice\ coefficient = \frac{TP \times 2}{TP \times 2 + FP + FN} \quad (12)$$

$$Jacard = \frac{TP}{TP+FP+FN} \quad (13)$$

Where, TP is the true positive; TN is the true negative; FP is a false positive and FN is a false negative.

4.1 Performance evaluation for SLSIBIF-MSVM

The performance of the SLSIBIF-MSVM method is analyzed for segmentation and classification. For segmentation results, the SLSIBIF is analyzed with different segmentation approaches such as Level set, saliency, saliency-Fuzzy C Means (FCM) clustering and Saliency level set without improvisation (SLSWD). The segmented output image of SLSIBIF along with the conventional segmentation approaches are shown in Table 1.

The segmentation results of different skin cancer classes such as nevus, seborrheic keratosis and

Table 2. Segmentation results of nevus

Methods	Jacard (%)	Dice (%)	Accuracy (%)	Sensitivity (%)
Level set	57.57	63.93	67.38	48.91
Saliency	74.59	48.79	40.97	39.87
Saliency-FCM	49.99	69.12	80.44	55.88
SLSWI	42.97	72.63	85.70	57.03
SLSIBIF	10.98	94.19	96.35	89.02

Table 3. Segmentation results of seborrheic keratosis

Methods	Jacard (%)	Dice (%)	Accuracy (%)	Sensitivity (%)
Level set	65.00	40.00	80.00	28.00
Saliency	78.00	21.00	67.00	34.00
Saliency-FCM	63.00	44.00	82.00	35.00
SLSWI	69.75	46.44	93.59	30.25
SLSIBIF	25.23	85.57	97.68	74.83

Table 4. Segmentation results of melanoma

Methods	Jacard (%)	Dice (%)	Accuracy (%)	Sensitivity (%)
Level set	67.00	46.00	79.00	68.00
Saliency	75.00	34.00	56.00	47.00
Saliency-FCM	45.00	67.00	80.63	70.43
SLSWI	26.59	84.67	93.46	73.41
SLSIBIF	18.75	89.66	95.39	81.25

Table 5. Average segmentation results of all classes

Methods	Jacard (%)	Dice (%)	Accuracy (%)	Sensitivity (%)
Level set	63.19	49.98	75.46	48.30
Saliency	75.86	34.60	54.66	40.29
Saliency-FCM	52.66	60.04	81.02	53.77
SLSWI	46.44	67.92	90.92	53.56
SLSIBIF	18.32	89.80	96.47	81.70

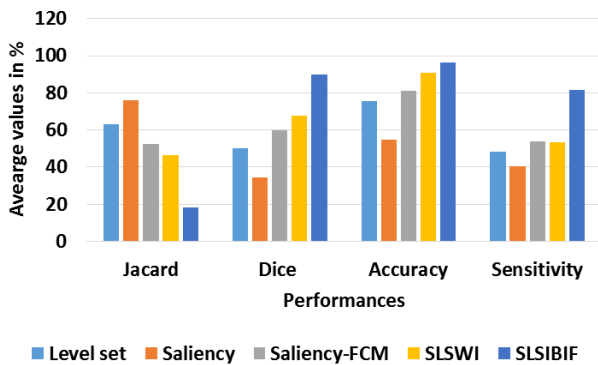


Figure. 3 Graphical illustration of average segmentation results for different segmentation approaches

melanoma are shown in Tables 2, 3, and 4 respectively. From Tables 2 to 4, it is identified that the SLSIBIF achieved better segmentation than the Level set, saliency, saliency-FCM clustering and SLSWI. Further, the average segmentation results for all classes are shown in Table 5 and Fig. 3. For example, the average accuracy of SLSIBIF for segmentation is 96.47% whereas the Level set obtains 75.46%, saliency obtains 54.66%, saliency-FCM

obtains 81.02% and SLSWI obtains 90.92%. The developed SLSIBIF provides better segmentation, because of the integration of both the saliency and LSF with an improved boundary indicator. This improved boundary indicator is used to perform an effective segmentation by avoiding issues related to illumination and low intensity.

The classification results of SLSIBIF-MSVM are analyzed with some conventional classifiers K nearest neighbor (KNN), random forest (RF) and decision tree (DE). The analysis of classification results for SLSIBIF-MSVM with KNN, RF and DE is shown in Table 6. Further, the graphical illustration of classification results for SLSIBIF-MSVM with KNN, RF and DE is shown in Fig. 4. This analysis shows that the MSVM achieves better results than the KNN, RF, and DE. For example, the accuracy of SLSIBIF-MSVM is 98.74% whereas the KNN obtains 96.12%, RF obtains 96.46% and DE obtains 95.04%. The MSVM provides better classification results because it is effective in handling high-dimension spaces as well as controls non-linear issues.

Table 6. Analysis of classification results for SLSIBIF-MSVM

Classifiers	Accuracy (%)	Sensitivity (%)	Specificity (%)	PPV (%)	Error-rate (%)
KNN	96.12	96.39	97.07	96.09	3.88
RF	96.46	93.22	95.20	94.25	3.54
DE	95.04	96.20	94.01	93.05	4.96
SLSIBIF-MSVM	98.74	98.89	99.40	98.36	1.26

Table 7. K-fold analysis of SLSIBIF-MSVM

K-fold values	Classifiers	Accuracy (%)	Sensitivity (%)	Specificity (%)	PPV (%)	Error-rate (%)
4 (Validation training 75% testing 25%)	KNN	95.09	94.56	93.07	96.25	4.91
	RF	95.40	96.40	94.95	93.22	4.60
	DE	93.36	94.37	95.71	92.35	6.64
	MSVM	97.82	95.79	97.80	96.21	2.18
5 (Validation training 80% testing 20%)	KNN	96.12	96.39	97.07	96.09	3.88
	RF	96.46	93.22	95.20	94.25	3.54
	DE	95.04	96.20	94.01	93.05	4.96
	MSVM	98.74	98.68	99.40	98.36	1.26
7 (Validation training 86% testing 24%)	KNN	95.25	93.37	95.68	93.96	4.75
	RF	94.98	92.68	95.31	91.21	5.02
	DE	94.89	94.88	93.35	92.82	5.11
	MSVM	98.25	96.60	96.63	98.29	1.75
9 (Validation training 88.5% testing 21.5%)	KNN	95.97	94.89	93.75	92.17	4.03
	RF	93.90	90.19	89.80	91.93	6.10
	DE	93.19	92.78	93.69	90.38	6.81
	MSVM	97.90	96.92	98.95	98.19	2.11
10 (Validation training 90% testing 10%)	KNN	94.05	93.95	91.39	90.34	5.95
	RF	92.99	90.58	89.75	92.63	7.01
	DE	92.93	91.63	93.70	94.02	7.07
	MSVM	98.11	96.23	98.11	96.74	1.89

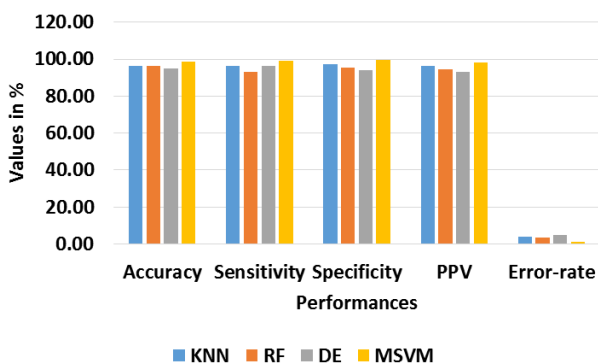


Figure. 4 Graphical illustration of classification results for different classifiers

The K-fold analysis of SLSIBIF-MSVM with different classifiers such as KNN, RF and DE is shown in Table 7. In this analysis, different K-fold values such as 4 (Validation training 75% testing 25%), 5 (Validation training 80% testing 20%), 7 (Validation training 86% testing 24%), 9 (Validation training 88.5% testing 21.5%) and 10 (Validation training 90% testing 10%) are taken for the analysis purpose. This analysis shows that the K-fold with a value of 5 achieves better results than the remaining variations.

4.2 Comparative analysis

The comparative analysis is done for three different datasets ISIC-2016, ISIC-2017 and PH2. The number of data exist in the ISIC-2016, ISIC-2017 and PH2 are 1250, 2750 and 200 images. The ISIC-2016 and PH2 are considered in this comparison to prove that SLSIBIF-MSVM outperforms well even with less amount of data. Here, the SLSIBIF-MSVM is evaluated with the DLS [17], ResNet-50 [18], K means GOA [19] and RCNN-FKM [20] based on the datasets which are analysed in their researches. The comparison of ISIC-2016, ISIC-2017 and PH2 datasets for SLSIBIF-MSVM are shown in Table 8, 9 and 10 respectively. From Tables 8-10, it is concluded that the SLSIBIF-MSVM outperforms well than the DLS [17], ResNet-50 [18], K means GOA [19] and RCNN-FKM [20]. The developed SLSIBIF provides better segmentation, because of the integration of both the saliency and LSF with an improved boundary indicator. This improved boundary indicator is used to perform an effective segmentation by avoiding issues related to illumination and low intensity.

Table 8. Comparative analysis for ISIC-2016 dataset

Methods	Accuracy (%)
DLS [17]	97.49
ResNet-50 [18]	79.95
RCNN-FKM [20]	95.4
SLSIBIF-MSVM	98.89

Table 9. Comparative analysis for ISIC-2017 dataset

Methods	Accuracy (%)
DLS [17]	97.94
ResNet-50 [18]	81.57
K means GOA [19]	98.42
RCNN-FKM [20]	95.2
SLSIBIF-MSVM	98.74

Table 10. Comparative analysis for PH2 dataset

Methods	Accuracy (%)
DLS [17]	97.23
K means GOA [19]	98.01
RCNN-FKM [20]	96.1
SLSIBIF-MSVM	98.73

5. Conclusion

In this research, the multi-class classification of skin cancer is improved by using an effective segmentation using SLSIBIF. The saliency and LSF are combined in the SLSIBIF along with an improved boundary indicator function to overcome the issues of illumination and low intensity during the segmentation. Since normalization is used as the pre-processing for improving the pixel intensity of input images by varying the pixel range. The GoogLeNet-based feature extraction obtains an appropriate feature by using sparse connections. Further, the MSVM is used to classify the multiple classes of skin cancer. Therefore, an effective segmentation using SLSIBIF improves skin cancer classification. From the results, it is concluded that the developed SLSIBIF-MSVM provides better performance than the DLS, ResNet-50, K means GOA and RCNN-FKM. The classification accuracy of SLSIBIF-MSVM for ISIC-2017 dataset is 98.74%, which is high when compared to the DLS, ResNet-50, K means GOA and RCNN-FKM.

Conflicts of interest

The authors declare no conflict of interest.

Author contributions

The paper conceptualization, methodology, software, validation, formal analysis, investigation, resources, data curation, writing—original draft preparation, writing—review and editing, visualization, have been done by 1st author. The

supervision and project administration, have been done by 2nd author.

References

- [1] H. C. Reis, V. Turk, K. Khoshelham, and S. Kaya, "InSiNet: a deep convolutional approach to skin cancer detection and segmentation", *Medical & Biological Engineering & Computing*, Vol. 60, No. 3, pp. 643-662, 2022.
- [2] M. S. Ali, M. S. Miah, J. Haque, M. M. Rahman, and M. K. Islam, "An enhanced technique of skin cancer classification using deep convolutional neural network with transfer learning models", *Machine Learning with Applications*, Vol. 5, p. 100036, 2021.
- [3] P. P. Tumpa and M. A. Kabir, "An artificial neural network based detection and classification of melanoma skin cancer using hybrid texture features", *Sensors International*, Vol. 2, p. 100128, 2021.
- [4] M. Toğaçar, Z. Cömert, and B. Ergen, "Intelligent skin cancer detection applying autoencoder, MobileNetV2 and spiking neural networks", *Chaos, Solitons & Fractals*, Vol. 144, p. 110714, 2021.
- [5] S. S. Chaturvedi, J. V. Tembhrne, and T. Diwan, "A multi-class skin Cancer classification using deep convolutional neural networks", *Multimedia Tools and Applications*, Vol. 79, No. 39, pp. 28477-28498, 2020.
- [6] M. A. Kassem, K. M. Hosny, and M. M. Fouad, "Skin lesions classification into eight classes for ISIC 2019 using deep convolutional neural network and transfer learning", *IEEE Access*, Vol. 8, pp. 114822-114832, 2020.
- [7] V. Anand, S. Gupta, A. Altameem, S. R. Nayak, R. C. Poonia, and A. K. J. Saudagar, "An Enhanced Transfer Learning Based Classification for Diagnosis of Skin Cancer", *Diagnostics*, Vol. 12, No. 7, p. 1628, 2022.
- [8] M. Fraiwan and E. Faouri, "On the Automatic Detection and Classification of Skin Cancer Using Deep Transfer Learning", *Sensors*, Vol. 22, No. 13, p. 4963, 2022.
- [9] C. Xin, Z. Liu, K. Zhao, L. Miao, Y. Ma, X. Zhu, Q. Zhou, S. Wang, L. Li, F. Yang, and S. Xu, "An improved transformer network for skin cancer classification", *Computers in Biology and Medicine*, Vol. 149, p. 105939, 2022.
- [10] Q. Chen, M. Li, C. Chen, P. Zhou, X. Lv, and C. Chen, "MDFNet: application of multimodal fusion method based on skin image and clinical

- data to skin cancer classification”, *Journal of Cancer Research and Clinical Oncology*, 2022.
- [11] S. Aladhadh, M. Alsanea, M. Aloraini, T. Khan, S. Habib, and M. Islam, “An Effective Skin Cancer Classification Mechanism via Medical Vision Transformer”, *Sensors*, Vol. 22, No. 11, p. 4008, 2022.
- [12] M. A. Khan, M. Sharif, T. Akram, S. Kadry, and C. H. Hsu, “A two-stream deep neural network-based intelligent system for complex skin cancer types classification”, *International Journal of Intelligent Systems*, Vol. 37, No. 12, pp. 10621-49, 2022.
- [13] M. K. Monika, N. A. Vignesh, C. U. Kumari, K. N. V. S. S. Kumar, and E. L. Lydia, “Skin cancer detection and classification using machine learning”, *Materials Today: Proceedings*, Vol. 33, pp. 4266-4270, 2020.
- [14] T. Saba, “Computer vision for microscopic skin cancer diagnosis using handcrafted and non-handcrafted features”, *Microscopy Research and Technique*, Vol. 84, No. 6, pp. 1272-1283, 2021.
- [15] M. Y. Yacin, B. A. Alrasheadi, N. B. Prakash, G. R. Hemalakshmi, A. Mohanarathinam, and K. Shankar, “Deep learning based an automated skin lesion segmentation and intelligent classification model”, *Journal of Ambient Intelligence And Humanized Computing*, Vol. 12, No. 3, pp. 3245-3255, 2021.
- [16] A. A. Teodoro, D. H. Silva, R. L. Rosa, M. Saadi, L. Wuttisittikulij, R. A. Mumtaz, and D. Z. Rodríguez, “A Skin Cancer Classification Approach using GAN and RoI-Based Attention Mechanism”, *Journal of Signal Processing Systems*, 2022.
- [17] S. Khoulood, M. Ahlem, T. Fadel, and S. Amel, “W-net and inception residual network for skin lesion segmentation and classification”, *Applied Intelligence*, Vol. 52, No. 4, pp. 3976-3994, 2022.
- [18] M. A. A. Masni, D. H. Kim, and T. S. Kim, “Multiple skin lesions diagnostics via integrated deep convolutional networks for segmentation and classification”, *Computer Methods and Programs in Biomedicine*, Vol. 190, p. 105351, 2020.
- [19] P. Thapar, M. Rakhra, G. Cazzato, and M. S. Hossain, “A novel hybrid deep learning approach for skin lesion segmentation and classification”, *Journal of Healthcare Engineering*, Vol. 2022, No. 1709842, 2022.
- [20] M. Nawaz, Z. Mehmood, T. Nazir, R. A. Naqvi, A. Rehman, M. Iqbal, and T. Saba, “Skin cancer detection from dermoscopic images using deep learning and fuzzy k-means clustering”, *Microscopy Research and Technique*, Vol. 85, No. 1, pp. 339-351, 2022.
- [21] N. C. Codella, D. Gutman, M. E. Celebi, B. Helba, M. A. Marchetti, S. W. Dusza, A. Kalloo, K. Liopyris, N. Mishra, H. Kittler, and A. Halpern, “Skin lesion analysis toward melanoma detection: A challenge at the 2017 international symposium on biomedical imaging (ISBI), hosted by the international skin imaging collaboration (ISIC)”, In: *Proc. of 2018 IEEE 15th International Symposium on Biomedical Imaging (ISBI 2018)*, Washington, DC, USA, IEEE, pp. 168-172, April 2018.
- [22] M. Zhang, Y. Yuan, R. Wang, and W. Cheng, “Recognition of mixture control chart patterns based on fusion feature reduction and fireworks algorithm-optimized MSVM”, *Pattern Analysis and Applications*, Vol. 23, No. 1, pp. 15-26, 2020.